Inorg. Chem. **2008**, *47*, 5245−5252

Reversible Redox-Switchable Second-Order Optical Nonlinearity in Polyoxometalate: A Quantum Chemical Study of $[PW_{11}O_{39}(ReN)]^{n-}$ ($n = 3-7$)

Wei Guan, Guochun Yang, Chunguang Liu, Ping Song, Liang Fang, Likai Yan, and Zhongmin Su*

Institute of Functional Material Chemistry, Faculty of Chemistry, Northeast Normal University, Changchun 130024, P. R. China

Received January 24, 2008

In this paper, the relationship between the reversible redox properties and the second-order nonlinear optical (NLO) responses for the title series of complexes has been systematically investigated by using the time-dependent density functional theory (TDDFT) method combined with the sum-over-states (SOS) formalism. The results reveal that the successive reduction processes of five $PW_{11}ReN$ redox states should be $PW_{11}Re^{VII}$ (**1**) → $PW_{11}Re^{VI}$ (**2**) → $PW_{11}Re^{V}$ (**3**) → $PW_{11}Re^{V}1e$ (**4**) → $PW_{11}Re^{V}2e$ (**5**). Furthermore, their electrochemical properties have been reproduced successfully. It is noteworthy that the second-order NLO behaviors can be switched by reversible redox for the present studied complexes. Full oxidation constitutes a convenient way to switch off the second-order polarizability (system **1**). The incorporation of extra electrons causes significant enhancement in the second-order NLO activity, especially for the third reduced state (system **4**), whose static second-order polarizability (β_{vec}) is about 144 times larger than that of fully oxidized **1**. The characteristic of the charge-transfer transition corresponding to the dominant contributions to the β_{vec} values indicates that metal-centered redox processes influence the intramolecular donor or acceptor character. Therefore, these kinds of complexes with the facile and reversible redox states could become excellent switchable NLO materials.

Introduction

Polyoxometalates (POMs) have constituted a rich class of molecular metal−oxygen clusters and exhibit remarkable chemical, physical, and biological properties, which have been applied to a variety of fields including catalysis, medicine, magnetism, optics, conductivity, and so forth.[1] However, in most cases, the practical applications of POMs in many areas depend on their redox properties, photochemical response, ionic charge, and so forth.[2] Most of them are related to one inherent characteristic of POMs, which is the special ability to be reduced by one or several excess electrons without significantly deforming the POM framework.[3] POMs as electron acceptors enable the formation of hybrid materials in which delocalized electrons coexist in both the organic network and the inorganic clusters. Such materials not only combine the advantages of organic materials so as to realize the so-called value-adding properties but also contribute to exploring the possible synergistic effects. Over the past few years, considerable efforts have been directed toward the nitride or organoimido functionalization of redox-active closed-framework POMs.[1j] The groups of Errington, Maatta, and Peng independently established oxo metathesis routes to the organoimido-functionalized hexamolybdate and achieved a lot of excellent results.[4] Recently, Wei and co-workers synthesized oragnoimido-functionalized hexamolybdate dimers via dehydrogenative coupling of primary amines with α-$[Mo_8O_{26}]^{4-}$.[5] As the potential of Keggin or Dawson over Lindqvist POM-based molecular materials should be greater, the functionalization of Keggin-type POMs has attracted much attention from both the experimental and theoretical chemistry fields. Proust et al. synthesized three nitrido-functionalized Keggin-type heteropolyanions, $[PW_{11}O_{39}\{Re^{VI}N\}]^{4-}$, $[PW_{11}O_{39}\{Re^{VII}N\}]^{3-}$, and $[PW_{11}O_{39}\{Os^{VI}N\}]^{4-}$, which illustrate the first time that rhenium- and osmium-nitrido were inserted into the POMs.[6] Subsequently, the rhenium phenylimido tungstophosphate, $[PW_{11}O_{39}\{Re^{V}NC_6H_5\}]^{4-}$, was prepared.[7] Duhacek and Duncan reported recently an organoimido-functionalized iso-addenda tungstophosphate, $[PW_{12}O_{39}\{NC_6H_5\}]^{3-}$.[8] Moreover, the elec-

* To whom correspondence should be addressed. Fax: 86-431-85684009. E-mail: zmsu@nenu.edu.cn.

10.1021/ic8001527 CCC: $40.75
Published on Web 05/21/2008

tronic and redox properties of $[PW_{11}O_{39}\{ReN\}]^{n-}$ ($n = 3, 4, 5$) and $[PW_{11}O_{39}\{Os^{VIII}N\}]^{2-}$ have been studied with density functional theory (DFT) by our group.[3e]

Nonlinear optical (NLO) materials based on molecular compounds have continued to be of considerable current interest because they hold promise for potential applications in optical signal processing, telecommunications, optical computing, and so forth. The incorporation of switchability into the NLO behavior of such materials will further increase their potential for novel applications in emerging optoelectronic and photonic technologies.[9] The NLO behavior may be switched using several methods, such as photoisomerization,[10] phototautomerizaton,[11] and phototcyclization.[12] Nevertheless, the most attractive procedures involve redox manipulation, since it may be easier to achieve in solid-state devices. Coe et al. used the redox switching of the Ru metal center to design various switchable NLO compounds.[13] Other workers subsequently reported the similar effects for both quadratic and cubic optical nonlinearities.[14] Nevertheless, NLO studies based on the reversible redox property are relatively lacking at present, especially theoretical works. To achieve a pronounced switching effect, the molecule must be stable in two (or more) states that exhibit very different NLO responses. Complete reversibility and high switching speed are also highly desirable for practical applications. Most POMs can be sufficient to these needs due to their extensive and reversible redox chemistry. Furthermore, experimental and theoretical investigations have shown that POM-based hybrid complexes hold a remarkably large NLO response.[15] This fact inspired us to further investigate the NLO properties of POM-based derivatives by theoretical computation. Quantum chemical calculations can be very helpful to experimental chemists who synthesize and test NLO materials, in the establishment of structure−property relationships as well as the elucidation of mechanisms involved in the generation of NLO activity. The aim of this article is to combine attractive redox properties and the NLO response of POM anions to obtain switchable NLO materials. As shown in previous experimental studies, $PW_{11}ReN$ possesses four one-electron reversible redox waves.[6] To analyze the relationship between the redox properties and the second-order NLO responses, we report a detailed DFT study on the five redox states of nitrido-functionalized Keggin-type heteropolyanions $[PW_{11}O_{39}\{ReN\}]^{3-}$ (**1**), $[PW_{11}O_{39}\{ReN\}]^{4-}$ (**2**), $[PW_{11}O_{39}\{ReN\}]^{5-}$ (**3**), $[PW_{11}O_{39}\{ReN\}]^{6-}$ (**4**), and $[PW_{11}O_{39}\{ReN\}]^{7-}$ (**5**). It is shown that the NLO activity can be controlled by one-electron redox processes. As the molecular NLO field matures, it can be anticipated that POM materials which exhibit switchable NLO properties will find various novel applications.

(1) (a) Pope, M. T. *Heteropoly and Isopoly Oxometalates*; Springer-Verlag: Berlin, 1983. (b) Pope, M. T.; Müller, A. *Angew. Chem., Int. Ed. Engl.* **1991**, *30*, 34–48. (c) Pope, M. T.; Müller, A. *Polyoxometalates: From Platonic Solid to Anti-Retroviral Activity*; Kluwer, Dordrecht, the Netherlands, 1994. (d) Hill, C. L.; Prosser-McCartha, C. M. *Coord. Chem. Rev.* **1995**, *143*, 407–455. (e) Hill, C. L. *Chem. Rev.* **1998**, *98*, special issue. (f) Müller, A.; Kögerler, P. *Coord. Chem. Rev.* **1999**, *182*, 3–17. (g) Kazansky, L. P.; McGarvey, B. R. *Coord. Chem. Rev.* **1999**, *188*, 157–210. (h) Clemente-Juan, J. M.; Coronado, E. *Coord. Chem. Rev.* **1999**, 193–195; 361−394. (i) Proust, A. *Actual. Chim.* **2000**, *7*−*8*, 55–61. (j) Pope, M. T.; Müller, A. *Polyoxometalate Chemistry: From Topology via Self-Assembly to Applications*; Kluwer: Dordrecht, The Netherlands, 2001. (k) Casañ-Pastor, N.; Gomez-Romero, P. *Front. Biosci.* **2004**, *9*, 1759–1770. (l) Coronado, E.; Giménez-Saiz, C.; Gómez-García, C. J. *Coord. Chem. Rev.* **2005**, *249*, 1776–1796. (m) Mizuno, N.; Yamaguchi, K.; Kamata, K. *Coord. Chem. Rev.* **2005**, *249*, 1944–1956. (n) Hasenknopf, B. *Front. Biosci.* **2005**, *10*, 275–287. (o) Yin, C. X.; Sasaki, Y.; Finke, R. G. *Inorg. Chem.* **2005**, *44*, 8521–8530. (p) Gong, Y.; Hu, C. W.; Liang, H. *Prog. Nat. Sci.* **2005**, *15*, 385–394. (q) Xie, Y. B. *Nanotechnology* **2006**, *17*, 3340–3346. (r) Xie, Y. B. *Adv. Funct. Mater.* **2006**, *16*, 1823–1831. (s) Long, D. L.; Burkholder, E.; Cronin, L. *Chem. Soc. Rev.* **2007**, *36*, 105–121.

(2) Katsoulis, D. E. *Chem. Rev.* **1998**, *98*, 359–387.

(3) (a) Maestre, J. M.; López, X.; Bo, C.; Poblet, J. M.; Casañ-Pastor, N. *J. Am. Chem. Soc.* **2001**, *123*, 3749–3758. (b) López, X.; Bo, C.; Poblet, J. M. *J. Am. Chem. Soc.* **2002**, *124*, 12574–12582. (c) Duclusaud, H.; Borshch, S. A. *J. Am. Chem. Soc.* **2001**, *123*, 2825–2829. (d) Guan, W.; Yan, L. K.; Su, Z. M.; Liu, S. X.; Zhang, M.; Wang, X. H. *Inorg. Chem.* **2005**, *44*, 100–107. (e) Yan, L. K.; Dou, Z.; Guan, W.; Shi, S. Q.; Su, Z. M. *Eur. J. Inorg. Chem.* **2006**, 5126–5129.

(4) (a) Clegg, W.; Errington, R. J.; Fraser, K. A.; Holmes, S. A.; Schäfer, A. *Chem. Commun.* **1995**, 455–456. (b) Du, Y. H.; Rheingold, A. L.; Maatta, E. A. *J. Am. Chem. Soc.* **1992**, *114*, 345–346. (c) Strong, J. B.; Yap, G. P. A.; Ostrander, R.; Liable-Sands, L. M.; Rheingold, A. L.; Thouvenot, R.; Gouzerh, P.; Maatta, E. A. *J. Am. Chem. Soc.* **2000**, *122*, 639–649. (d) Wei, Y. G.; Xu, B. B.; Barnes, C. L.; Peng, Z. H. *J. Am. Chem. Soc.* **2001**, *123*, 4083–4084. (e) Xu, L.; Lu, M.; Xu, B. B.; Wei, Y. G.; Peng, Z. H.; Powell, D. R. *Angew. Chem., Int. Ed.* **2002**, *41*, 4129–4132.

(5) Li, Q.; Wei, Y. G.; Hao, J.; Zhu, Y. L.; Wang, L. S. *J. Am. Chem. Soc.* **2007**, *129*, 5810–5811.

(6) (a) Kwen, H.; Tomlinson, S.; Maatta, E. A.; Dablemont, C.; Thouvenot, R.; Proust, A.; Gouzerh, P. *Chem. Commun.* **2002**, 2970–2971. (b) Dablemont, C.; Hamaker, C. G.; Thouvenot, R.; Sojka, Z.; Che, M.; Maatta, E. A.; Proust, A. *Chem.*−*Eur. J.* **2006**, *12*, 9150–9160.

(7) Dablemont, C.; Proust, A.; Thouvenot, R.; Afonso, C.; Fournier, F.; Tabet, J.-C. *Inorg. Chem.* **2004**, *43*, 3514–3520.

(8) Duhacek, J. C.; Duncan, D. C. *Inorg. Chem.* **2007**, *46*, 7253–7255.

(9) (a) Lehn, J.-M. *Supramolecular Chemistry Concepts and Perspectives*; VCH: Weinheim, Germany, 1995. (b) Coe, B. J. *Chem.*−*Eur. J.* **1999**, *5*, 2464–2471. (c) Asselberghs, I.; Clays, K.; Persoons, A.; Ward, M. D.; McCleverty, J. A. *J. Mater. Chem.* **2004**, *14*, 2831–2839. (d) Coe, B. J. *Acc. Chem. Res.* **2006**, *39*, 383–393.

(10) Loucif-Saïbi, R.; Nakatani, K.; Delaire, J. A.; Dumont, M.; Sekkat, Z. *Chem. Mater.* **1993**, *5*, 229–236.

(11) Nakatani, K.; Delaire, J. A. *Chem. Mater.* **1997**, *9*, 2682–2684.

(12) (a) Gilat, S. L.; Kawai, S. H.; Lehn, J.-M. *Chem.*−*Eur. J.* **1995**, *1*, 275–284. (b) Fernandez-Acebes, A.; Lehn, J.-M. *Chem.*−*Eur. J.* **1999**, *5*, 3285–3292.

(13) (a) Coe, B. J.; Houbrechts, S.; Asselberghs, I.; Persoons, A. *Angew. Chem., Int. Ed.* **1999**, *38*, 366–369. (b) Coe, B. J.; Harris, J. A.; Jones, L. A.; Brunschwig, B. S.; Song, K.; Clays, K.; Garín, J.; Orduna, J.; Coles, S. J.; Hursthouse, M. B. *J. Am. Chem. Soc.* **2005**, *127*, 4845–4859.

(14) (a) Weyland, T.; Ledoux, I.; Brasselet, S.; Zyss, J.; Lapinte, C. *Organometallics* **2000**, *19*, 5235–5237. (b) Malaun, M.; Reeves, Z. R.; Paul, R. L.; Jeffery, J. C.; McCleverty, J. A.; Ward, M. D.; Asselberghs, I.; Clays, K.; Persoons, A. *Chem. Commun.* **2001**, 49–50. (c) Cifuentes, M. P.; Powell, C. E.; Humphrey, M. G.; Heath, G. A.; Samoc, M.; Luther-Davies, B. *J. Phys. Chem. A* **2001**, *105*, 9625–9627. (d) Hurst, S. K.; Cifuentes, M. P.; Morrall, J. P. L.; Lucas, N. T.; Whittall, I. R.; Humphrey, M. G.; Asselberghs, I.; Persoons, A.; Samoc, M.; Luther-Davies, B.; Willis, A. C. *Organometallics* **2002**, *20*, 4664–4675. (e) Paul, F.; Costuas, K.; Ledoux, I.; Deveau, S.; Zyss, J.; Halet, J.-F.; Lapinte, C. *Organometallics* **2002**, *21*, 5229–5235. (f) Asselberghs, I.; Clays, K.; Persoons, A.; McDonagh, A. M.; Ward, M. D.; McCleverty, J. A. *Chem. Phys. Lett.* **2003**, *368*, 408–411. (g) Sortino, S.; Petralia, S.; Bella, S. D. *J. Am. Chem. Soc.* **2003**, *125*, 5610–5611. (h) Sporer, C.; Ratera, I.; Ruiz-Molina, D.; Zhao, Y.-X.; Vidal-Gancedo, J.; Wurst, K.; Jaitner, P.; Clays, K.; Persoons, A.; Rovira, C.; Veciana, J. *Angew. Chem., Int. Ed.* **2004**, *43*, 5266–5268. (i) Dalton, G. T.; Cifuentes, M. P.; Petrie, S.; Stranger, R.; Humphrey, M. G.; Samoc, M. *J. Am. Chem. Soc.* **2007**, *129*, 11882–11883.

Computational Details

DFT calculations were carried out using the Amsterdam Density Functional (ADF) program.[16] Electron correlation was treated within the local density approximation (LDA) in the Vosko−Wilk−Nusair parametrization.[17] The nonlocal corrections of Becke[18] and Perdew[19] were added to the exchange and correlation energies, respectively. The basis functions for describing the valence electrons of each atom are triple-ζ plus polarization Slater-type orbitals, which are standard TZP basis sets in the ADF package. The core shells {O, N: $(1s)^2$; P: $(1s2s2p)^{10}$; W, Re: $(1s2s2p3s3p3d4s4p4d)^{46}$} were kept frozen and were described by means of single Slater functions. The zero-order regular approximation was adopted in all of the calculations to account for the scalar relativistic effects.[20] To reduce the discrepancy between the gas-phase calculation and the solution-phase measurement, the solvent effects were employed in the calculations of geometry optimization and excitation properties by using a conductor-like screening model (COSMO)[21] of solvation with the solvent-excluding surface.[22] The solute dielectric constant was set to 37.5 (acetonitrile). The van der Waals radii for the POM atoms, which actually define the cavity in the COSMO, are 1.41, 1.40, 1.92, 2.10, and 2.17 Å for N, O, P, W, and Re, respectively.[23] Full geometry optimizations (assuming C_1 symmetry) were carried out on each complex both in the gas phase and in solution. Spin-unrestricted calculations were performed for all of the considered open-shell systems.

Time-dependent density functional theory (TDDFT) is one of the most popular methods for the calculation of excitation properties in quantum chemistry due to its efficiency and accuracy. It has been used to study the electron spectra of numerous systems, including closed- and open-shell systems. By far, the accuracy and reliability of spin-unrestricted TDDFT for open-shell systems have been tested by studying both the organic and transition metal compounds.[24] To elucidate and analyze the effect of reduction on the second-order NLO properties of the present studied systems, the EXCITATION modules[25] implemented in the ADF program were used on the basis of the optimized geometries in the gas phase and in solution. All of the calculations of excitation properties were based on the van Leeuwen−Baerends XC potential (LB94).[26] The adiabatic local density approximation was applied for the evaluation of the first and second functional derivatives of the XC potential. Spin-unrestricted TDDFT calculations were adopted and performed for all of the considered open-shell systems. Moreover, the value of the numerical integration parameter used to determine the precision of numerical integrals was 6.0.

Then, the second-order polarizabilities were calculated by using the sum-over-states (SOS) formula.[27] The expression of the second-order polarizabilities' β tensors can be obtained by the application of time-dependent perturbation theory to the interacting electromagnetic field and microscopic system. The zeroth-order Born−Oppenheimer approximation was also employed to separate the electronic and atomic components of β. The expression for β_{ijk} is

$$\beta_{ijk} = \frac{1}{4\hbar^2} P(i,j,k;-\omega_\sigma,\omega_1,\omega_2) \times \sum_{m\neq g}\sum_{n\neq g}\left[\frac{(\mu_i)_{gm}(\bar{\mu}_j)_{mn}(\mu_k)_{ng}}{(\omega_{mg}+\omega_\sigma-i\gamma_{mg})(\omega_{ng}-\omega_1-i\gamma_{ng})}\right] \quad (1)$$

where $(\mu_i)_{gm}$ is an electronic transition moment along the i axis of the Cartesian system, between the ground state and the excited state, $(\bar{\mu}_j)_{mn}$ is the dipole difference equal to $(\mu_i)_{mn} - (\mu_i)_{gg}$, ω_{mg} is the transition energy, ω_1 and ω_2 are the frequencies of the perturbation radiation fields, and $\omega_\sigma = \omega_1 + \omega_2$ is the polarization response frequency; $P(i,j,k;-\omega_\sigma,\omega_1,\omega_2)$ indicates all permutations of ω_1, ω_2, and ω_σ along with associated indices i, j, and k; γ_{mg} is the damping factor. We self-compiled a program using the results of TDDFT and the SOS formula to obtain the second-order polarizabilities, and we have used this method to investigate the NLO properties of a series of compounds.[15g,24k,28]

In addition, to further interpret the bonding character between rhenium and nitrogen, a natural bond orbital (NBO) calculation at the B3LYP level was performed through the use of the Gaussian

(15) (a) Niu, J. Y.; You, X. Z.; Duan, C. Y.; Fun, H. K.; Zhou, Z. Y. *Inorg. Chem.* **1996**, *35*, 4211–4217. (b) Xu, X. X.; You, X. Z.; Huang, X. Y. *Polyhedron* **1995**, *14*, 1815–1824. (c) Zhang, M. M.; Shan, B. Z.; Duan, C. Y.; You, X. Z. *Chem. Commun.* **1997**, 1131–1132. (d) Murakami, H.; Kozeki, T.; Suzuki, Y.; Ono, S.; Ohtake, H.; Sarukura, N.; Ishikawa, E.; Yamase, T. *Appl. Phys. Lett.* **2001**, *79*, 3564–3566. (e) Xu, L.; Wang, E. B.; Li, Z.; Kurth, D. G.; Du, X. G.; Zhang, H. Y.; Qin, C. *New J. Chem.* **2002**, *26*, 782–786. (f) Yan, L. K.; Yang, G. C.; Guan, W.; Su, Z. M.; Wang, R. S. *J. Phys. Chem. B* **2005**, *109*, 22332–22336. (g) Yang, G. C.; Guan, W.; Yan, L. K.; Su, Z. M.; Xu, L.; Wang, E. B. *J. Phys. Chem. B* **2006**, *110*, 23092–23098. (h) Guan, W.; Yang, G. C.; Yan, L. K.; Su, Z. M. *Inorg. Chem.* **2006**, *45*, 7864–7868. (i) Guan, W.; Yang, G. C.; Yan, L. K.; Su, Z. M. *Eur. J. Inorg. Chem.* **2006**, 4179–4183.

(16) (a) te Velde, G.; Bickelhaupt, F. M.; Baerends, E. J.; Fonseca Guerra, C.; van Gisbergen, S. J. A.; Snijders, J. G.; Ziegler, T. *J. Comput. Chem.* **2001**, *22*, 931–967. (b) Fonseca Guerra, C.; Snijders, J. G.; te Velde, G.; Baerends, E. J. *Theor. Chem. Acc.* **1998**, *99*, 391–403. (c) *ADF 2006. 01*; SCM, Vrije Universiteit: Amsterdam, The Netherlands. http://www.scm.com (accessed May 2008).

(17) Vosko, S. D.; Wilk, L.; Nusair, M. *Can. J. Chem.* **1980**, *58*, 1200–1211.

(18) Becke, A. D. *Phys. Rev. A: At., Mol., Opt. Phys.* **1988**, *38*, 3098–3100.

(19) Perdew, J. P. *Phys. Rev. B: Condens. Matter Mater. Phys.* **1986**, *33*, 8822–8824.

(20) van Lenthe, E.; Baerends, E. J.; Snijders, J. G. *J. Chem. Phys.* **1993**, *99*, 4597–4610.

(21) (a) Klamt, A.; Schüürmann, G. *J. Chem. Soc., Perkin Trans.* **1993**, *2*, 799–805. (b) Klamt, A. *J. Chem. Phys.* **1995**, *99*, 2224–2235. (c) Klamt, A.; Jones, V. *J. Chem. Phys.* **1996**, *105*, 9972–9981. (d) Pye, C. C.; Ziegler, T. *Theor. Chem. Acc.* **1999**, *101*, 396–408.

(22) Pascualahuir, J. L.; Silla, E.; Tunon, I. *J. Comput. Chem.* **1994**, *15*, 1127–1138.

(23) Hu, S. Z.; Zhou, Z. H.; Tsai, K. R. *Wuli Huaxue Xuebao* **2003**, *19*, 1073–1077.

(24) (a) Hirata, S.; Head-Gordon, M. *Chem. Phys. Lett.* **1999**, *302*, 375–382. (b) Hirata, S.; Head-Gordon, M. *Chem. Phys. Lett.* **1999**, *314*, 291–299. (c) Spielfieldel, A.; Handy, N. C. *Phys. Chem. Chem. Phys.* **1999**, *1*, 2401–2409. (d) Adamo, C.; Barone, V. *Chem. Phys. Lett.* **1999**, *314*, 152–157. (e) Guan, J.; Casida, M. E.; Salahub, D. R. *THEOCHEM* **2000**, *527*, 229–244. (f) Broclawik, E.; Borowski, T. *Chem. Phys. Lett.* **2001**, *339*, 433–437. (g) Dai, B.; Deng, K. M.; Yang, J. L.; Zhu, Q. S. *J. Chem. Phys.* **2003**, *118*, 9608–9613. (h) Nemykin, V. N.; Basu, P. *Inorg. Chem.* **2003**, *42*, 4046–4056. (i) Wang, F.; Ziegler, T. *Mol. Phys.* **2004**, *104*, 2585–2595. (j) Hennig, H.; Schumer, F.; Reinhold, J.; Kaden, H.; Oelssner, W.; Schroth, W.; Spitzner, R.; Hartl, F. *J. Phys. Chem. A* **2006**, *110*, 2039–2044. (k) Yang, G. C.; Fang, L.; Tan, K.; Shi, S. Q.; Su, Z. M.; Wang, R. S. *Organometallics* **2007**, *26*, 2082–2087.

(25) van Gisbergen, S. J. A.; Snijders, J. G.; Baerends, E. J. *Comput. Phys. Commun.* **1999**, *118*, 119–138.

(26) van Leeuwen, R.; Baerends, E. J. *Phys. Rev. A: At., Mol., Opt. Phys.* **1994**, *49*, 2421–2431.

(27) Orr, B. J.; Ward, J. F. *Mol. Phys.* **1971**, *20*, 513–526.

(28) (a) Yang, G. C.; Qin, C. S.; Su, Z. M.; Shi, D. *THEOCHEM* **2005**, *726*, 61–65. (b) Yang, G. C.; Shi, D.; Su, Z. M.; Qin, C. S. *Acta Chim. Sinica* **2005**, *63*, 184–188. (c) Yang, G. C.; Su, Z. M.; Qin, C. S. *J. Phys. Chem. A* **2006**, *110*, 4817–4821. (d) Yang, G. C.; Liao, Y.; Su, Z. M.; Zhang, H. Y.; Wang, Y. *J. Phys. Chem. A* **2006**, *110*, 8758–8762. (e) Yang, G. C.; Shi, S. Q.; Guan, W.; Fang, L.; Su, Z. M. *THEOCHEM* **2006**, *773*, 9–14.

Table 1. Calculated Relative Energies ΔE (in kcal/mol) at Various Spin Multiplicities for Systems 3, 4, and 5 in the Gas Phase and in Solution

system	3		4		5		
spin multiplicity	1	3	2	4	1	3	5
ΔE (gas)	0.00	7.57	0.00	9.11	0.00	1.37	12.3
ΔE (acetonitrile)	0.00	7.66	0.00	8.11	0.00	1.08	11.7

03 suite of programs[29] based on the optimized geometries in solution. The basis set used for N, O, and P is the standard Gaussian basis set 6-31G(d), in which one set of d-polarization functions is included. For 5d transition metals, the Stuttgart/Dresden effective core potential basis set (SDD)[30] was used.

Results and Discussion

The Ground States. Because transition metal rhenium possesses unfilled d orbitals, it therefore can form various spin configurations. The optimized calculations were first performed at various possible spin multiplicities in order to find the structure with the lowest energy for each studied complex. In the following paper, we will use term "ground state" for the structure with the lowest energy. For closed-shell system **1**, the ground state is obviously from the singlet state. The ground state of system **2** has only one unpaired electron and thus a doublet state. Table 1 lists the calculated relative energies at various spin multiplicities for systems **3**, **4**, and **5** both in the gas phase and in solution. For spin-unrestricted calculations, the calculated square of total spin is quite close to its eigenvalues $s(s + 1)$, indicating that the spin contamination is minor (see the Supporting Information). As shown in the Table 1, it can be seen that, for systems **3**−**5**, the ground states were found. The ground state for system **3** is the singlet state that lies below the triplet state by 7.57 kcal/mol in the gas phase and 7.66 kcal/mol in acetonitrile. There are also two electronic configurations for system **4**; the doublet state is much more stable than the quartet state. For system **5**, the singlet state was calculated to be more stable than the triplet state, but the energy difference between the two configurations is relatively small, 1.37 kcal/mol in the gas phase and 1.08 kcal/mol in acetonitrile. The quintet state is more than 10 kcal/mol higher in energy than the ground state both in the gas phase and in acetonitrile, so it is quite unstable. Hence, the results reported in the following sections are based on the ground states for the studied systems.

(29) Frisch, M. J.; Trucks, G. W.; Schlegel, H. B.; Scuseria, G. E.; Robb, M. A.; Cheeseman, J. R.; Montgomery, J. A., Jr.; Vreven, T.; Kudin, K. N.; Burant, J. C.; Millam, J. M.; Iyengar, S. S.; Tomasi, J.; Barone, V.; Mennucci, B.; Cossi, M.; Scalmani, G.; Rega, N.; Petersson, G. A.; Nakatsuji, H.; Hada, M.; Ehara, M.; Toyota, K.; Fukuda, R.; Hasegawa, J.; Ishida, M.; Nakajima, T.; Honda, Y.; Kitao, O.; Nakai, H.; Klene, M.; Li, X.; Knox, J. E.; Hratchian, H. P.; Cross, J. B.; Adamo, C.; Jaramillo, J.; Gomperts, R.; Stratmann, R. E.; Yazyev, O.; Austin, A. J.; Cammi, R.; Pomelli, C.; Ochterski, J. W.; Ayala, P. Y.; Morokuma, K.; Voth, G. A.; Salvador, P.; Dannenberg, J. J.; Zakrzewski, V. G.; Dapprich, S.; Daniels, A. D.; Strain, M. C.; Farkas, O.; Malick, D. K.; Rabuck, A. D.; Raghavachari, K.; Foresman, J. B.; Ortiz, J. V.; Cui, Q.; Baboul, A. G.; Clifford, S.; Cioslowski, J.; Stefanov, B. B.; Liu, G.; Liashenko, A.; Piskorz, P.; Komaromi, I.; Martin, R. L.; Fox, D. J.; Keith, T.; Al-Laham, M. A.; Peng, C. Y.; Nanayakkara, A.; Challacombe, M.; Gill, P. M. W.; Johnson, B.; Chen, W.; Wong, M. W.; Gonzalez, C.; Pople, J. A. *Gaussian 03*, Revision C.02; Gaussian, Inc.: Pittsburgh PA, 2003.
(30) Andrae, D.; Haussermann, U.; Dolg, M.; Stoll, H.; Preuss, H. *Theor. Chim. Acta* **1990**, *77*, 123–141.

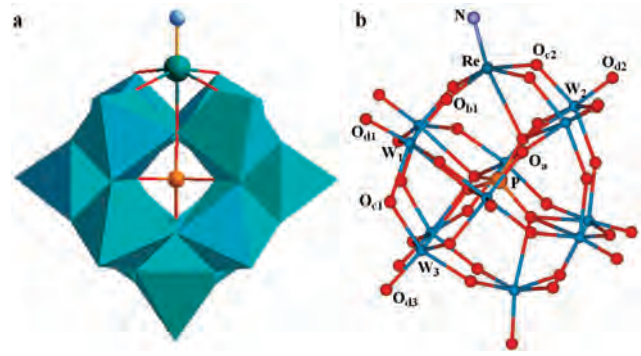

Figure 1. Polyhedral and ball-and-stick representations of calculation model $PW_{11}ReN$.

Molecular Structures. The Keggin-type hetero-polyanion is made of an assembly of 12 MO_6 octahedrons sharing their corners or edges with a central XO_4 tetrahedron (Figure 1a). The oxygen atoms in the Keggin framework can be divided into three categories: center tetrahedral oxygen (O_a), bridge oxygen (O_b and O_c), and terminal oxygen (O_d). The bridge oxygen can be divided into the corner-sharing oxygen of M_3O_{10} corner-sharing triads, O_b, and the corner-sharing oxygen of M_3O_{10} edge-sharing triads, O_c (Figure 1b). The selected bond distances for a series of optimized complexes are shown in Table 2. Most of the bond distances increase through successive one-electron reductions. It indicates that the reduction processes are accompanied by an expansion of the framework.[3e] Compared with the gas calculations, there is a generalized shortening (improvement) of the bond distances caused by the solvent effects. Moreover, as the negative charge of the heteropolyanion increases, the geometry is affected more obviously by the solvent effects.

However, the bond distances of Re—N almost keep constant in the reduction process. This strong interaction between rhenium and nitrogen agrees with the Re≡N triple-bond character reported by the experiments.[6] To further interpret the bonding character of Re≡N, we preformed NBO calculations on five $PW_{11}ReN$ complexes. For simplicity, Table 3 lists selected natural bond orbitals, occupancy, orbital coefficients and hybrids, and the orbital types of system **1** (for other systems, see the Supporting Information). NBO analysis reveals that the Re≡N triple bond is composed of a Re—N σ bond and two Re—N π bonds. Take system **1** for example, the σ bond is formed by a Re ($sd^{3.13}$) orbital and a N ($sp^{3.67}$) orbital, while the two π bonds are made up of a hybrid Re orbital and a pure p-N orbital, respectively. The other reduced systems also possess similar Re≡N triple-bond character. Furthermore, it is noticeable that the interaction between rhenium and nitrogen becomes stronger and stronger by the incorporation of extra electrons from the standpoint of the Wiberg bond index of Re≡N (see the Supporting Information). The strong interaction has been utilized to prepare the POM-based hybrid complexes.[7] In contrast, large deviations in the Re—O bonds are observed for the first two reductions from Table 2, while the bonds are approximately constant for the last two reductions. NBO results show a consistent change law based on the Wiberg bond indexes of Re—O_{b1} and Re—O_{c2} (see the Supporting Information). In

Table 2. The Selected Bond Distances (in Å) of Systems 1−5 Computed in the Gas Phase and in Solution

	1		2		3		4		5	
	gas	acetonitrile	gas	acetonitrile	gas	acetonitrile	gas	acetonitrile	gas	acetonitrile
Re−N	1.679	1.678	1.680	1.677	1.681	1.673	1.692	1.679	1.698	1.682
Re−O_{b1}	1.939	1.939	1.982	1.981	1.994	1.987	1.994	1.986	1.996	1.983
Re−O_{c2}	1.930	1.930	1.983	1.981	2.009	2.003	2.012	2.004	2.012	2.003
W_1−O_{b1}	1.921	1.920	1.875	1.873	1.850	1.849	1.867	1.862	1.874	1.873
W_1−O_{d1}	1.726	1.725	1.735	1.734	1.743	1.734	1.755	1.741	1.763	1.745
W_1−O_{c1}	1.943	1.943	1.979	1.977	2.017	2.012	2.012	2.006	2.000	1.993
W_2−O_{c2}	1.953	1.953	1.897	1.896	1.866	1.867	1.877	1.879	1.893	1.895
W_2−O_{d2}	1.726	1.726	1.733	1.732	1.745	1.733	1.754	1.741	1.763	1.745
W_3−O_{c1}	1.939	1.938	1.918	1.916	1.903	1.904	1.911	1.908	1.918	1.913
W_3−O_{d3}	1.725	1.725	1.734	1.732	1.747	1.732	1.756	1.740	1.760	1.742

Table 3. The Selected Natural Bond Orbitals, Occupancy, Orbital Coefficients and Hybrids, and Orbital Type of System 1

natural bond orbitals	occupancy	orbital coefficients and hybrids	orbital type
Re−N	1.95	0.63 $(sd^{3.13})_{Re}$ + 0.78 $(sp^{3.67})_N$	σ
Re−N	1.63	0.63 $(pd^{2.33})_{Re}$ + 0.78 $(p)_N$	π
Re−N	1.64	0.63 $(pd^{2.58})_{Re}$ + 0.78 $(p)_N$	π

fact, the change of metal-centered redox-active sites should be the basic cause of this phenomenon.

Redox Properties. As shown in a previous theoretical study, the rhenium−nitrido fragment appears to display a crucial effect upon the electronic properties of Keggin-type heteropolyanions.[3e] Changes of the electronic properties are related to the occupied orbitals, and they also affect the lowest unoccupied orbitals, thus leading to the change in the redox properties of these complexes. To shed further light on the redox properties for this kind of nitrido-functionalized Keggin-type heteropolyanion, we have systematically investigated various possible redox states both in the gas phase and in solution. When calculations are carried out in the gas phase, the frontier molecular orbitals usually have positive energies, but in solution, they are strongly stabilized by the effect of the solvent.[31] Figure 2 shows the frontier molecular orbital distribution for five $PW_{11}ReN$ redox states in acetonitrile. The highest occupied molecular orbital (HOMO) in fully oxidized **1** formally delocalizes over bridge oxygens and partially on the nitrogen atom, while the lowest unoccupied molecular orbital (LUMO) delocalizes mostly over d-rhenium orbitals at 39%, and d-tungsten orbitals account for about 15%, which is quite different from that of phosphotungstate.[3d] The LUMO+1 in system **1** concentrates on tungstens and slightly on bridge oxygen atoms. Hence, it suggests that the first reduction of system **1** should take place preferentially at the d-rhenium orbitals. The second reduction can occur at two possible sites, the rhenium center (β-LUMO in system **2**) or the tungsten centers (α-LUMO in system **2**). The energy difference between the two possibilities was calculated to be ~7.6 kcal/mol (Table 1). Different behavior was found when the third and fourth reductions occurred. It is seen that, in accord with the frontier molecular orbital distribution in Figure 2 and the analysis of the ground states mentioned above, tungsten atoms will become the reduced center when system **1** reaches the third or fourth reduction process. The Mülliken spin populations confirm these qualitative predictions. Table 4 lists the spin density distribution for systems **2** and **4** (similar values both in the gas phase and in acetonitrile). It shows that most of the spin density (0.67) in system **2** is localized on the Re atom, while the rest of the cage atoms (W, N, and O) together carry a small spin density. So, the first- and second-reduction process of system **1** is $PW_{11}Re^{VII}$ (**1**) → $PW_{11}Re^{VI}$ (**2**) → $PW_{11}Re^{V}$ (**3**), which fully agrees with previous experimental and theoretical studies.[3e,6] By contrast, W atoms in system **4** carry more spin density, which is in accord with the frontier molecular orbital in Figure 2. This suggests that W atoms have a greater ability to capture an extra electron than the Re atom in the third reduction process. From Table 4, the extra electron in system **4** is delocalized among the tungsten centers, so the reduction of system **3** will yield the blue species $PW_{11}Re^{V}1e$ (**4**) but not $PW_{11}Re^{IV}$. The same behavior occurs in system **5**. Hence, the third- and fourth-reduction process of system **1** should be $PW_{11}Re^{V}$ (**3**) → $PW_{11}Re^{V}1e$ (**4**) → $PW_{11}Re^{V}2e$ (**5**). However, this reduction process is different from the successive reductions of Re^{V} → Re^{IV} → Re^{III} reported in the experiments.[6]

On the basis of having established the reductive centers, we proceed to reproduce the electrochemical behavior of the present studied complexes. It has been proved that the oxidation−reduction potentials can be predicted theoretically in solution.[32] The theoretical prediction of the redox potentials of a given POM requires the determination of the free energy associated with the process.

$$PW_{11}Re_{Nox}\,(aq) + e^- \xrightarrow[\Delta G]{} PW_{11}ReN_{red}\,(aq) \qquad (2)$$

The term ΔG represents the free energy of the reduction process in solution. To proceed to compute ΔG, we must know the entropy, which has electronic, translational, rotational, and vibrational components. Since frequency calculations for these large systems will take an extremely

(31) (a) Romo, S.; Fernández, J. A.; Maestre, J. M.; Keita, B.; Nadjo, L.; de Graaf, C.; Poblet, J. M. *Inorg. Chem.* **2007**, *46*, 4022–4027. (b) Fernández, J. A.; López, X.; Bo, C.; de Graaf, C.; Baerends, E. J.; Poblet, J. M. *J. Am. Chem. Soc.* **2007**, *129*, 12244–12253.

(32) (a) Winget, P.; Weber, E. J.; Cramer, C. J.; Truhlar, D. G. *Phys. Chem. Chem. Phys.* **2000**, *2*, 1231–1239. (b) Baik, M.-H.; Silverman, J. S.; Yang, I. V.; Ropp, P. A.; Szalai, V. A.; Yang, W. T.; Thorp, H. H. *J. Phys. Chem. B* **2001**, *105*, 6437–6444. (c) Patterson, E. V.; Cramer, C. J.; Truhlar, D. G. *J. Am. Chem. Soc.* **2001**, *123*, 2025–2031. (d) Baik, M.-H.; Friesner, R. A. *J. Phys. Chem. A* **2002**, *106*, 7407–7412. (e) Arnold, W. A.; Winget, P.; Cramer, C. J. *Environ. Sci. Technol.* **2002**, *36*, 3536–3541. (f) Fu, Y.; Liu, L.; Yu, H. Z.; Wang, Y. M.; Guo, Q. X. *J. Am. Chem. Soc.* **2005**, *127*, 7227–7234. (g) Fu, Y.; Liu, L.; Wang, Y. M.; Li, J. N.; Yu, T. Q.; Guo, Q. X. *J. Phys. Chem. A* **2006**, *110*, 5874–5886.

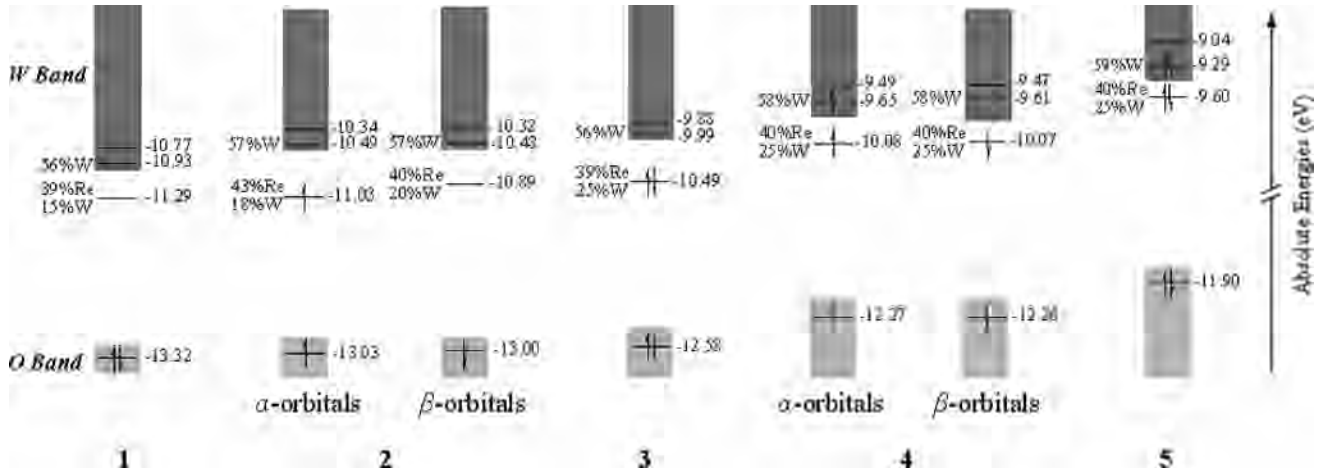

Figure 2. The frontier molecular orbital diagram for the studied complexes in acetonitrile.

Table 4. The Selected Spin Density Distribution of Systems 2 and 4 Computed in Acetonitrile

	Re	N	W_1	W_2	W_3	O_{b1}	O_{c1}	O_{c2}	O_{d1}	O_{d2}	O_{d3}
2	0.67	−0.09	0.04	0.04	0.00	0.01	0.01	0.02	−0.00	−0.00	−0.00
4	−0.03	0.00	0.12	0.12	0.12	0.01	−0.01	0.01	−0.01	−0.01	−0.01

Table 5. Comparison of Calculated (E_{cal}) and Experimental (E_{pc}) Reduction Potentials[a] (in V) versus SCE in Acetonitrile for the Studied Complexes

	1st reduction peak	2nd reduction peak	3rd reduction peak	4th reduction peak
E_{pc}	0.47	−0.49	−1.46	−1.92
E_{cal}	0.10	−0.45	−1.24	−1.60

[a] Experimental values obtained from ref 6b.

long time, some approximations have to be introduced. Neglect of the entropic term turns out to be mild due to very large electronic contributions for these charged POM species.[31] Therefore, ΔG can be approximated by the reduction energy of the complex in solution. The free energy change associated with the reference normal hydrogen electrode half-reaction has been recalculated to be −4.36 V.[33] So the reference saturated calomel electrode (SCE) should be −4.60 V. When the Nernst equation $E° = -\Delta G°/nF$ is combined with the reference value −4.60 V, the reduction potentials (E_{cal}) can be predicted. Table 5 summarizes calculated reduction potentials and experimental reduction potentials versus SCE. It can be seen that the theoretical predications agree with the experimental data. The discrepancy between the E_{pc} values and the E_{cal} values may be modified by considering the protonation of the complexes in the reduction processes.[31]

Second-Order Polarizabilities. The incorporation of extra electrons results in a certain influence on geometries and electronic properties of $PW_{11}ReN$ complexes, which inspired us to further investigate the effect of reduction on second-order NLO properties using the TDDFT method combined with the SOS formalism. Compared with the gas calculations, the calculated spectra with the solvent effect could impact the excitations not only in energies but in the intensities, so the results reported in the following text are based on the calculations considering the solvent effect (for a detailed comparison, see the Supporting Information). The accuracy of the SOS method mainly depends on the convergence of calculation results. According to the convergent curves (see the Supporting Information), employing 100 states in the present work is a reasonable approximation in the calculation of β values.

The static second-order polarizability (β_{vec}) is termed as the zero-frequency hyperpolarizability and is an estimate of the intrinsic molecular hyperpolarizability in the absence of a resonance effect. The calculated results reveal a strong dependence of the β_{vec} values upon the redox states of $PW_{11}ReN$ complexes. As can be seen from Figure 3, the reduced complexes show more than 30 times the efficiency of fully oxidized **1**. This indicates that the incorporation of extra electrons causes significant enhancement in the molecular nonlinearity. However, the β_{vec} values of $PW_{11}ReN$ complexes do not increase monotonically with successive one-electron reductions. The maximum β_{vec} value (-15.83×10^{-30} esu) appears when the third reduction occurs. It is about 144 times larger than the β_{vec} value of fully oxidized **1**. The computed β_{vec} values of systems **2**−**4** show that the NLO response is the following: system **4** > system **3** > system **2**. The β_{vec} value of system **4** is about twice as large

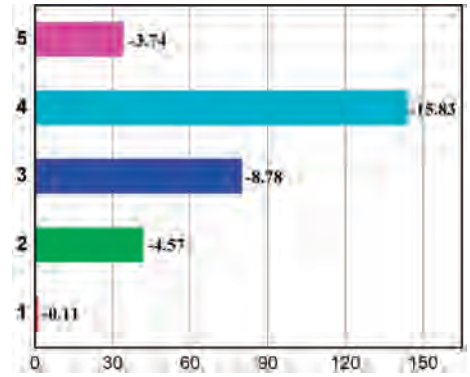

Figure 3. Comparison of the static β_{vec} (1×10^{-30} esu) values for the studied systems.

(33) Lewis, A.; Bumpus, J. A.; Truhlar, D. G.; Cramer, C. J. *J. Chem. Educ.* **2004**, *81*, 596–603.

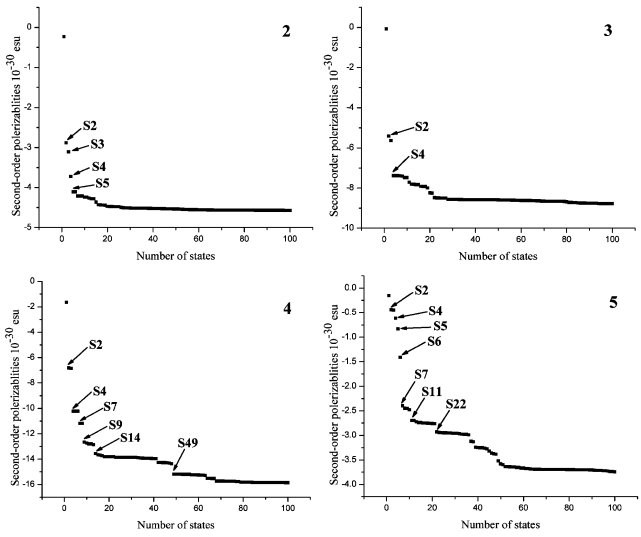

Figure 4. Plots of static β_{vec} values as computed in the SOS formalism as a function of the number of excited states for systems **2**−**5**.

as that of system **3**, which, in turn, is about twice as large as that of system **2**. But the β_{vec} value of the fourth reduced system, **5**, drops by about 75% in comparison with that of system **4**. Therefore, these kinds of complexes with the reversible and manipulable redox states could become excellent switchable NLO materials.

In order to elucidate the origin of nonlinear second-order responsibilities of these complexes, we took a further step into several main excited states that contribute to the β_{vec} value. A really dominant contribution cannot be observed in the case of system **1**. It is clear that the two-level model is inappropriate for system **1**. However, from the frontier molecular orbital distribution for system **1** (Figure 2), p-oxygen orbital → d-rhenium orbital or p-oxygen orbital → d-tungsten orbital transitions should contribute largely to the β_{vec} value. For the reduced complexes, several main excited states can be seen from Figure 4. The excited state S2 has the dominant contribution to the β_{vec} value of system **2**; S3, S4, and S5 have comparative contributions. For system **3**, the excited states S2 and S4 have large contributions to the β_{vec} value, especially for S2. For systems **4** and **5**, the dominant contribution to β_{vec} values can be assigned to S2 and S4 and to S6 and S7, respectively. Other excited states have comparatively small contributions. TDDFT calculations indicate that system **4** has similar compositions between the excited states S2 and S4. The same phenomenon occurs between S6 and S7 for system **5**. Thus, the excited state S2 for systems **2**−**4** and S6 for system **5** should be paid more attention. As can be seen from Table 6, the excited state S2 for systems **2**−**4** is mainly made up of αHOMO → αLUMO+1, HOMO → LUMO+1, and αHOMO → αLUMO+1, respectively. The excited state S6 for system **5** is primarily composed of HOMO → LUMO+4. The corresponding molecular orbitals of these desired excited states are illustrated in Figure 5. It is obvious that transitions αHOMO → αLUMO+1 (**2**) and HOMO → LUMO+1 (**3**) can be assigned to the charge transfer from d-rhenium orbitals to d-tungsten orbitals; while the transitions αHOMO → αLUMO+1 (**4**) and HOMO → LUMO+4 (**5**) are equal to

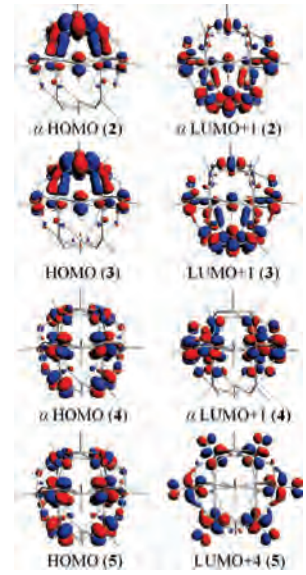

Figure 5. The corresponding molecular orbitals of the excited-state S2 for systems 2−4 and the excited-state S6 for system 5.

Table 6. The Corresponding Transition Energies (*E* in eV), Oscillator Strengths (*f*), and Dominant Transition of the Excited State S2 for Systems 2−4 and the Excited State S6 for System 5

system	excited state	*E*	*f*	major transition
2	S2	0.74701	0.0044	α HOMO → LUMO+1
3	S2	0.78116	0.0131	HOMO → LUMO+1
4	S2	0.31745	0.0013	α HOMO → LUMO+1
5	S6	0.73136	0.0057	HOMO → LUMO+4

the charge transfer between d-tungsten orbitals. These transition characteristics can provide information on the way metal-centered redox processes influence the intramolecular donor or acceptor character, which accordingly leads to the variations in the computed β_{vec} values. As can be found from Figures 2 and 5, the Re or W center acts as an acceptor and the oxo band acts as a donor in system **1**, whereas the Re center becomes a donor and the W centers act as an acceptor in systems **2** and **3**. For systems **4** and **5**, the W centers possess both donor and acceptor character.

Why is there the strong dependence of the β_{vec} values upon the redox states of $PW_{11}ReN$ complexes? From the complex SOS expression, the two-level model that linked between β and a low-lying charge-transfer transition has been established.[34] For the static case, the following model expression is employed to estimate β_{CT}:

$$\beta_{CT} \propto \frac{\Delta\mu_{gm} f_{gm}}{E_{gm}^3} \tag{3}$$

where f_{gm}, E_{gm}, and $\Delta\mu_{gm}$ are the oscillator strength, the transition energy, and the difference of the dipole moment between the ground state (g) and the *m*th excited state (*m*), respectively. In the two-level model expression, the second-order polarizability caused by charge transfer, β_{CT}, is proportional to the optical intensity and is inversely proportional to the cube of the transition energy. Hence, for the studied complexes, the low excitation energy is the decisive

(34) (a) Oudar, J. L.; Chemla, D. S. *J. Chem. Phys.* **1977**, *66*, 2664. (b) Oudar, J. L. *J. Chem. Phys.* **1977**, *67*, 446–457.

factor in the β value. As can be seen from Table 6, system **4** has a much smaller excitation energy than other systems. The larger charge transfer will come into being under the external electronic field. In addition, there are more relatively larger contributions to the β_{vec} value (Figure 4). These behaviors can explain why the maximum β_{vec} value appears at the third reduction. The computed E values of other systems are comparable; however, the f value of system **3** is largest, which is helpful to enhance the β_{vec} value. For the rest, changes of β_{vec} values can also be explained according to the analysis of the two-level model and the main contribution to the β_{vec} value. Thus, although the strict application of the two-level model might be questionable for the large and open-shell complexes investigated here, such a simple model still rationalizes our results on the basis of the corresponding transition energies and oscillator strengths of the desired excited states.

Conclusions

For the first time, a quantum chemical study of the relationship between the reversible redox properties and the second-order NLO responses has been performed on nitrido-functionalized Keggin-type POM species, $[PW_{11}O_{39}(ReN)]^{n-}$ ($n = 3-7$). From the optimized calculations at various possible spin multiplicities both in the gas phase and in acetonitrile, the ground state for each redox state can be found. NBO analysis confirms the Re≡N triple covalent bond that is composed of a Re—N σ bond and two Re—N π bonds and reveals that the interaction between rhenium and nitrogen becomes stronger and stronger with the incorporation of extra electrons from the standpoint of the Wiberg bond index of Re≡N. DFT calculations suggest that the successive reduction processes should be $PW_{11}Re^{VII}$ (**1**) → $PW_{11}Re^{VI}$ (**2**) → $PW_{11}Re^{V}$ (**3**) → $PW_{11}Re^{V}$1e (**4**) → $PW_{11}Re^{V}$2e (**5**). Furthermore, we have reproduced successfully the electrochemical behavior of the present studied complexes. Using TDDFT combined with the SOS method, we have shown that the second-order NLO behaviors can be switched by reversible redox for the present studied complexes. Full oxidation constitutes a convenient way to switch off the second-order polarizability. The incorporation of extra electrons causes significant enhancement in the second-order NLO activity, especially for the third reduced state (system **4**), whose static second-order polarizability (β_{vec}) is about 144 times larger than that of fully oxidized **1**. Analysis of the dominant contributions to the β_{vec} value suggests that, for system **1**, the second-order NLO response originates from p-oxygen orbital → d-rhenium orbital or p-oxygen orbital → d-tungsten orbital transitions, comparatively for systems **2** and **3**; the NLO responses arise from the charge transfer from d-rhenium orbitals to d-tungsten orbitals; in addition, the charge transfer between d-tungsten orbitals plays a key role in the NLO response of systems **4** and **5**. These transition characteristics indicate that metal-centered redox processes influence the intramolecular donor or acceptor character, which accordingly leads to the variations in the computed β_{vec} values. Therefore, these kinds of complexes with the facile and reversible redox states might conveniently be used for switching purposes in molecular devices for NLO.

Acknowledgment. The authors gratefully acknowledge the financial support from the National Natural Science Foundation of China (Project Nos. 20573016), the Training Fund of NENU'S Scientific Innovation Project (NENU-STC07017), and the Science Foundation for Young Teachers of Northeast Normal University (20070304) and are supported by the Program for Changjiang Scholars and Innovative Research Team in University (PCSIRT). We also thank YHK for computational support.

Supporting Information Available: Comparison between the exact and expectation value of the total spin for spin-unrestricted calculations, NBO calculated results of systems 2−5, computed electronic spectra both in the gas phase and in acetonitrile for systems 1−5, and convergent behaviors of the second-order polarizabilities for systems 1−5. This material is available free of charge via the Internet at http://pubs.acs.org.

IC8001527